

Quantum correlation of electron and ion energy in the dissociative strong-field ionization of H₂A. Geyer^{1,*}, O. Neufeld^{2,†}, D. Trabert¹, U. De Giovannini^{2,3}, M. Hofmann¹, N. Anders¹, L. Sarkadi⁴, M. S. Schöffler¹, L. Ph. H. Schmidt¹, A. Rubio^{2,5}, T. Jahnke⁶, M. Kunitski¹ and S. Eckart^{1,‡}¹*Institut für Kernphysik, Goethe-Universität, Max-von-Laue-Str. 1, 60438 Frankfurt am Main, Germany*²*Max Planck Institute for the Structure and Dynamics of Matter and Center for Free-Electron Laser Science, 22761 Hamburg, Germany*³*Università degli Studi di Palermo, Dipartimento di Fisica e Chimica - Emilio Segrè, via Archirafi 36, I-90123 Palermo, Italy*⁴*Institute for Nuclear Research (ATOMKI), P.O. Box 51, H-4001 Debrecen, Hungary*⁵*Center for Computational Quantum Physics (CCQ), The Flatiron Institute, New York, New York 10010, USA*⁶*European XFEL, Holzkoppel 4, 22869 Schenefeld, Germany*

(Received 12 May 2022; accepted 20 January 2023; published 16 February 2023)

We report on the strong field ionization of H₂ by a corotating two-color laser field. We measure the electron momentum distribution in coincidence with the kinetic energy release (KER) of dissociating hydrogen molecules. In addition to a characteristic half-moon structure, we observe a low-energy structure in the electron momentum distribution at a KER of about 3.5 eV. We speculate that the outgoing electron interacts with the molecular ion, despite the absence of classical recollisions under these conditions. Time-dependent density functional theory simulations support our conclusions.

DOI: [10.1103/PhysRevResearch.5.013123](https://doi.org/10.1103/PhysRevResearch.5.013123)

I. INTRODUCTION

Ionization of atoms and molecules in strong laser fields is often successfully modeled as a tunneling process [1]. After tunneling, the electron's trajectory is governed by the time-dependent laser electric field and the potential of the parent ion. Consequently, the time-dependent laser electric field can be used to control the trajectory of the liberated electron. For linearly polarized light or for suitable two-color laser fields the electron can exchange energy with its parent ion by inelastic recollisions. Examples for processes which are enabled by electrons that return to their parent ions are the recombination of the tunneled electron with its parent ion [2,3], which can lead to the emission of high order harmonics [4–6], excitation of the parent ion [7], or nonsequential double ionization [8–14]. Previous studies in the strong field regime observed such energy exchange only if the electron recollided with its parent ion during the photoionization process.

In this Letter, we report on the single ionization of molecular hydrogen by a corotating two-color (CoRTC) field accompanied by dissociation of the molecule: H₂ → H + H⁺ + e[−]. The CoRTC field is created as a superposition of two circularly polarized laser pulses with the same helicity

and central wavelengths of 790 nm and 390 nm. The intensity of the fundamental laser pulse (780 nm) and the second harmonic one (390 nm) were set to 3.3×10^{13} W/cm² and 5.4×10^{13} W/cm², respectively. The CoRTC field ensures that recollisions are negligible during the photoionization process [13,15,16]. The Lissajous curves of the laser electric field and the corresponding vector potential are depicted in Fig. 1(a). Figure 1(b) shows the projection of the measured three-dimensional (3D) electron momentum distribution to the polarization plane $p_y p_z$. As expected, the most probable electron momentum is close to the value of the negative vector potential that belongs to the peak of the electric laser field [17–19].

After one of the two bound electrons of H₂ is liberated, the electron's trajectory is governed by the driving laser electric field and the interaction with the H₂⁺ ion. The second electron remains bound in the energetically lowest molecular orbital (1σ_g) of H₂⁺ while the occupation of the antibinding orbital (2pσ_u) remains negligible. This scenario is ideally suited to study the interaction of the liberated electron with its parent molecular ion in strong field ionization. The molecular ion with its 1σ_g and 2pσ_u state can be approximated as a two-level system, which has an energy spacing that depends on the internuclear distance. Our results show evidence that the escaping electron drives an excitation in this two-level system by transferring a fraction of its energy to the H₂⁺ parent ion.

II. EXPERIMENT

A. Experimental method

In our experiment, the CoRTC field is generated by an interferometric two-color laser setup. Multicycle laser pulses

*geyer@atom.uni-frankfurt.de

†ofer.neufeld@mpsd.mpg.de

‡eckart@atom.uni-frankfurt.de

with a central wavelength of 780 nm, a pulse duration of 40-fs FWHM, and a repetition rate of 8 kHz (KMLabs Dragon) are frequency doubled in a β -barium borate crystal to create light pulses at a central wavelength of 390 nm. The two pulses with different wavelengths are spatially separated for independent modification of their polarization state and intensity. The relative phase between the two pulses is controlled using a nanometer-delay stage. A beam combiner merges the two single-color laser pulses. The two-color laser field is focused onto the H_2 target inside a vacuum chamber by a spherical mirror ($f = 80$ mm). The optical setup is the same as in Ref. [20].

The 3D electron and proton momenta are measured in coincidence using a COLTRIMS (cold target recoil ion momentum spectroscopy) reaction microscope as in Ref. [21]. The charged particles are accelerated by a homogeneous electric field of 17 Vcm^{-1} and a parallel magnetic field of 10 G onto position- and time-sensitive detectors [22]. The length of the electron spectrometer is 378 mm and the length of the ion spectrometer is 68 mm. Making use of momentum conservation, the detection of the proton and the electron allows for the calculation of the kinetic energy release $\text{KER} = \frac{(p_p + 0.5 \cdot p_e)^2}{m_p}$, where p_p and p_e are the momenta of the detected proton and electron, respectively, and m_p is the proton mass. The background from false coincidences and the contribution from events in which both electrons are liberated has been subtracted for all experimental data that are shown.

Measured electron momentum distributions from the ionization of argon by circularly polarized light are used to calibrate the laser intensity of the two colors separately. Thus, the intensity calibration has been done *in situ* and takes volume averaging into account. For the laser pulse at a central wavelength of 780 nm the drift momentum is used to calibrate the intensity taking nonadiabaticity into account as described in Ref. [20]. For the laser pulse at a central wavelength of 390 nm the shift of the above threshold ionization (ATI) peaks is used for intensity calibration as in Ref. [12]. The relative phase between the two colors, which determines the orientation of the combined electric field in the plane of polarization, was actively varied during the measurement. These variations are compensated during the offline data analysis as in Ref. [20].

B. Experimental results

The measured electron momentum distribution that is shown in Fig. 1(b) is very similar to previous findings for atoms [15,20,23]. In particular, the choice to investigate the reaction $H_2 \rightarrow H + H^+ + e^-$ enables us to resolve the measured electron momentum distribution as a function of the KER of the ions. The measured KER is shown in Fig. 2(a). The most probable KER is 1.2 eV. Figures 2(b)–2(d) show the 3D electron momentum distributions and the corresponding two-dimensional projections for three different KER ranges as indicated in Fig. 2(a). All electron momentum distributions show a characteristic half-moon structure. For a KER of about 3.5 eV, there additionally exists a pronounced low-energy structure. Such low-energy structures in CoRTC fields have been observed for atoms before [15] using different laser parameters [24]. However, the low-energy structure in our

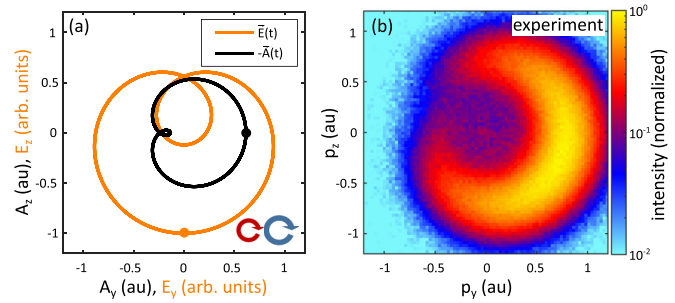


FIG. 1. (a) The Lissajous curve of the laser electric field and the corresponding negative vector potential. The arrows indicate the temporal evolution of the laser electric field. The dots indicate the peak of $|\vec{E}(t)|$ and the corresponding negative vector potential. (b) Measured electron momentum distribution for the laser field that is shown in (a) with a logarithmic color scale.

measurement solely becomes visible for a specific KER region and is not present for other KERs.

To further investigate the relation of electron energy and KER, Fig. 3(a) shows the correlated yield of these two quantities. Column-wise normalization of the data from Fig. 3(a) results in Fig. 3(b), which shows two remarkable correlations between the electron energy and the KER. Firstly, for $\text{KER} < 3 \text{ eV}$ we find diagonal structures spaced by 1.6 eV reflecting the quantized absorption of energy from the field. This ATI structure is well documented in the literature [25–27]. Further, the electron-nuclear sharing of the absorbed photon energy has already been investigated for H_2 [28,29] and other molecules [30,31]. The second feature is the appearance of the low energy electrons for a KER range of 3 eV to 6 eV. Within this region, the most probable electron energy is lower than that for a KER below 3 eV and there is a sharp edge at a KER of 3 eV. What is the reason for this correlation of KER and electron energy?

Figure 3(c) shows the potential energy curves for the ground state of H_2 , for a binding molecular orbital ($1s\sigma_g$), and an antibinding orbital ($2p\sigma_u$) of H_2^+ . The liberation of the first electron is indicated by a vertical arrow labeled with “two-color strong field ionization” in Fig. 3(c). The very pronounced KER peak at about 1.2 eV is reached via subsequent nuclear dynamics and absorption of a photon at 390 nm [21] (indicated with the arrow that is labeled “ 2ω ”). Analogous to the 2ω -peak at 1.2 eV, the KER peaks at 0.2 eV and 2.8 eV are caused by the absorption of one or three 780 nm photons. The net-two-photon pathway, which corresponds to an absorption of three 780 nm photons and a stimulated emission of one 780 nm photon [32], also leads to a KER peak at around 1.2 eV for our laser parameters. Thus, it overlaps with the 2ω -peak and is very weak, since this pathway is expected to be less probable than the three-photon peak for 780 nm at 2.8 eV. Hence, for the KER peaks below 3 eV, the reaction can be separated into two steps. The first step is the same as it would be for an atom: an electron is liberated and subsequently accelerated in the laser field. The final electron momentum p_e roughly corresponds to the negative vector potential at the instance of ionization $-\vec{A}(t_0)$. For close to circularly polarized light, the ponderomotive potential U_p is given by $U_p = \frac{p_e^2}{2m_e} =$

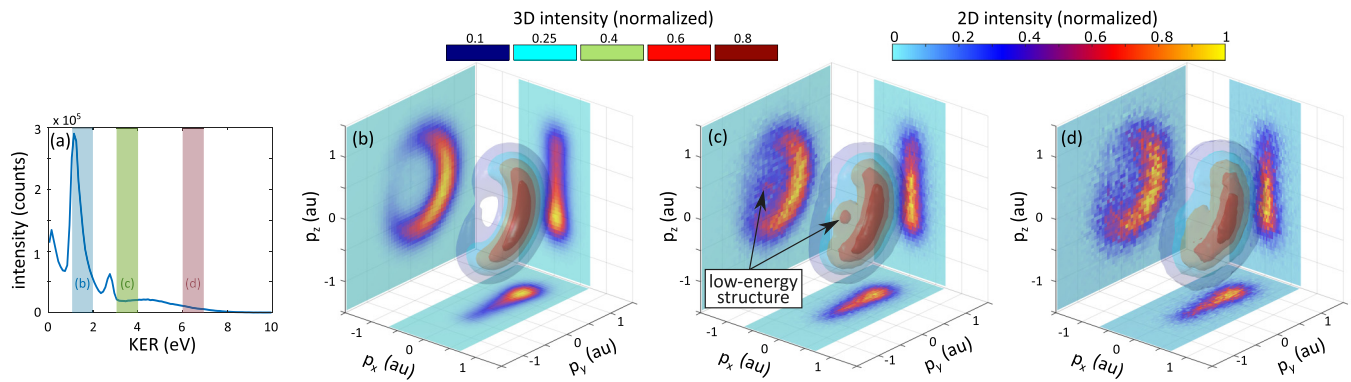


FIG. 2. (a) Shows the measured kinetic energy release (KER) distribution for the reaction $\text{H}_2 \rightarrow \text{H} + \text{H}^+ + e^-$. (b)–(d) show the measured electron momentum distributions which are restricted to the measured KER intervals that are indicated in (a). The three-dimensional (3D) electron momentum distributions are represented using five semitransparent isosurfaces encoding the intensity of the 3D histogram by color. The $p_y p_z$ plane is the polarization plane.

$e^2 \frac{|\vec{A}(t_0)|^2}{2m_e}$, where $m_e [e]$ is the electron's mass [charge]. For the time t_0 that belongs to the peak electric field, this leads to a value of $U_p = 5.2 \text{ eV}$. Thus, the half-moon structure that is observed in the current experiment is, as expected, very

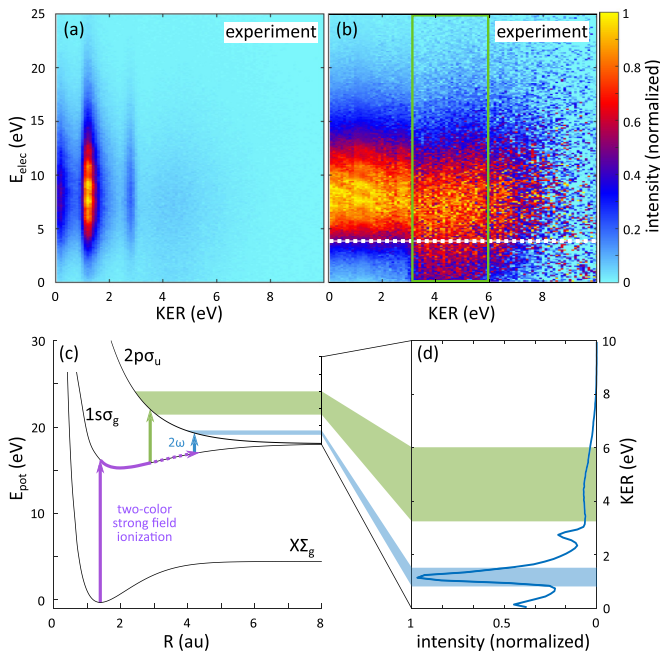


FIG. 3. Experimental data on the strong field dissociation of H_2 . (a) shows the energy of the electron as a function of the KER. In (b) each column of the distribution in (a) is normalized to a maximum of one. The horizontal line in (b) guides the eye and the green square highlights the KER region in which there is the low-energy structure. (b) reveals that low-energy electrons ($E_{\text{elec}} < 3 \text{ eV}$) are very pronounced for $3 \text{ eV} < \text{KER} < 6 \text{ eV}$. (c) shows the potential energy of the ground state of H_2 and two states of H_2^+ as a function of the internuclear distance. The purple arrow marks the strong field transition from the ground state to the $1s\sigma_g$ state. Two possible transitions from the $1s\sigma_g$ to the $2p\sigma_u$ curve are marked by a blue and a green arrow, respectively. The KERs that result from these two transitions are marked by colored areas in the KER distribution in (d). (d) shows the same data as Fig. 2(a).

similar as for the ionization of atoms [20]. In a second step, there can be subsequent nuclear dynamics which occur on a time scale of tens of femtoseconds [33,34].

Inspection of the potential energy curves in Fig. 3(c) suggest the following physical picture: the KER of around 3.5 eV , for which the low-energy structure is most prominent, indicates that the transition from the $1s\sigma_g$ state to the $2p\sigma_u$ state occurs at an internuclear distance of about $R = 3 \text{ a.u.}$ (neglecting the kinetic energy of the nuclear wave packet after the ionization step). At $R = 3 \text{ a.u.}$ the spacing between the $1s\sigma_g$ and the $2p\sigma_u$ state is 5.6 eV as indicated by the vertical green arrow in Fig. 3(c). Interestingly, this value for the energy splitting is very close to $U_p = 5.2 \text{ eV}$. In a first attempt, we tried to explain the electron-ion correlation as an energy transfer from the electron to the ion that occurs during a recollision. To this end, we have performed extensive modeling of classical dynamics including electron-electron interactions [35,36] and trajectories with nonzero initial electron momentum at the tunnel exit as predicted by SFA [20,37,38]. We have also modeled the molecular geometry and classical ionic motion during the photoionization process. None of these simulations yielded a significant amount of recolliding trajectories [12] with the required energy of at least 5 eV , or resulted in a substantial amount of low energy electrons. Thus, these simulations allow us to rule out classical electron-ion recollisions in our experiment, and verify that classical dynamics is not the source of the observed effect.

III. TIME-DEPENDENT DENSITY FUNCTIONAL THEORY

To further investigate the correlation of electron energy and KER we perform *ab initio* simulations that fully incorporate the ionization dynamics of electrons, as well as ion motion. The electronic degrees of freedom are treated quantum mechanically by time-dependent density functional theory (TDDFT) [39] within the local density approximation and the adiabatic approximation with an added self-interaction correction term that leads to the correct long-range Coulomb behavior [40]. This approach incorporates mean-field electron-electron interactions, as well as interactions of electrons with the incident laser fields, and nuclei. The

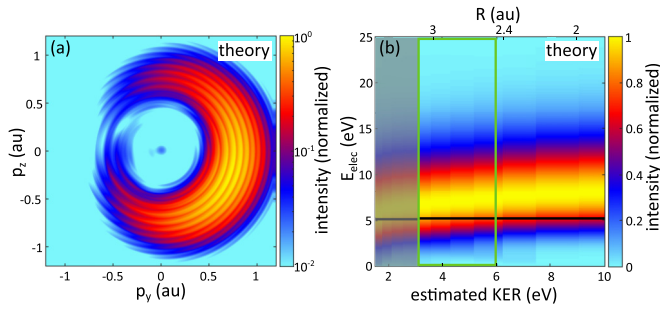


FIG. 4. Theoretical data on the ionization of H_2 in a CoRTC field. (a) shows the electron momentum distribution with a logarithmic color scale that is obtained using a time-dependent density functional theory (TDDFT) approach. (b) shows the ionization probability as a function of the final electron energy and the internuclear distance R (upper horizontal axis) of the H_2 molecule. ATI peaks were removed by applying a low-pass filter to the electron energy distribution. Each column of the distribution is normalized to a maximum of one. The lower horizontal axis shows the corresponding estimated KER, which is derived from the $2p\sigma_u$ curve (see text). The black line indicates the ponderomotive energy $U_p = 5.2$ eV. The green square highlights the same KER region as in Fig. 3(b).

nuclei motion is treated classically by coupling Newtonian equations of motion to TDDFT [41], such that ions are driven by interactions with the time-dependent electric field of the laser, neighboring ions, and the electrons' charge density (ion motion is initiated in the ground vibrational state of H_2). Most importantly, this approach allows for energy exchange and coupling between the ionic and electronic degrees of freedom through Coulomb interactions. The photoelectron spectra are calculated with the surface flux method, T-surff [42–44] employing the dipole approximation (velocity gauge). All calculations are performed with octopus code [45–47], and utilize a Cartesian grid with a spacing of 0.4 Bohr, and a spherical boundary shape with a radius of 45 Bohr. We use a complex absorbing potential (CAP) with a width of 15 Bohr (time step of 2.6 attoseconds). The photoelectron flux is calculated at the spatial onset of the CAP. Our calculations assume that the hydrogen molecule is aligned along the y axis, in the laser polarization plane (the result was seen largely independent of the molecular orientation). The simulation uses the same laser parameters as in the experiment with the difference that in the simulation a shorter pulse duration of nine femtoseconds (FWHM in intensity) is used (envelope's shape taken from Ref. [48]). The phase between the H_2 zero point energy vibration and the laser is averaged over. Figure 4(a) shows the calculated electron momentum distribution. The low-energy structure is reproduced and its relative yield of about 1% compared to the main half-moon lobe, is in agreement with the experiment [see Fig. 1(b)].

In a next step, the nuclei's coordinates are frozen in the TDDFT simulations, which implies that one uses an inaccurate internuclear distance for the ionization step, and a static internuclear distance for the modeling of the subsequent electron-ion interaction. This allows one to disentangle the role of electron-ion energy exchange, because it samples the contribution of a single ionic configuration to the photoemission process by using a well-defined internuclear

distance. Figure 4(b) shows the intensity as a function of the final electron energy and the internuclear distance R of the H_2 molecule. The lower horizontal axis shows the corresponding estimated KER, which is obtained by subtracting the energy of the $2p\sigma_u$ state for $R \rightarrow \infty$ from the energy of the $2p\sigma_u$ state for the internuclear distance that is used in the TDDFT simulations. To visualize the dependence of the envelope of the calculated electron energy distribution as a function of R , the ATI substructure has been smoothed using a low-pass filter. Strikingly, also in the TDDFT simulations, the electron energy depends on the internuclear distance. The black line in Fig. 4(b) shows the ponderomotive energy $U_p = 5.2$ eV. In a simple man's model [2], the peak of the electron energy spectrum is at $U_p = 5.2$ eV for circularly polarized light. If one takes Coulomb interaction and nonadiabatic offsets of the initial momentum distribution into account, the peak of the electron energy spectrum typically shifts to slightly higher energies [20]. We expect that these corrections to the simple man's model do not depend on the internuclear distance. Thus, we speculate that there is an electron-ion interaction that decelerates the outgoing electron for an internuclear distance of about 3 a.u. Such electron-ion correlations are inherently included in our TDDFT simulation. A full understanding of the microscopic mechanism that leads to the observed correlations of electron and ion energy is beyond the scope of the current work and warrants further research.

It is an important difference, as compared to the experiment, that in Fig. 4(b) all electrons are shown. In the experiment the measured electrons are detected in coincidence with ions that predominantly dissociate via the $2p\sigma_u$ state. However, TDDFT does not allow to distinguish the state of the ion (e.g., $1s\sigma_g$ and $2p\sigma_u$). As a result, the TDDFT result misses the characteristic peaks for KERs below 3 eV that are due to resonant coupling of $1s\sigma_g$ and $2p\sigma_u$, which is due to the absorption of photons from the driving laser field [32,49]. We expect, that the agreement of experiment and theory could be further improved, if the final states would be projected to the ionic $2p\sigma_u$ state, which is impossible using state-of-the-art approaches.

IV. DISCUSSION

A microscopic reason for the observed correlation of electron energy and KER might be electron-electron interactions [50]. We consider the excitation of the molecule to a neutral excited H_2 state and subsequently ionization via the $1s\sigma_g$ or the $2p\sigma_u$ state to be unlikely, given that the KER is above 3.5 eV and that the average electron energy increases with increasing KER (this is opposite to the expectation for energy sharing) [51]. Alternatively, we speculate that our observations might be related to an antenna-like mechanism [52,53]. If the ponderomotive energy U_p of the outgoing electron is resonant to the energy spacing of the $1s\sigma_g$ and the $2p\sigma_u$ state, then the electron can transfer this amount of energy to the H_2^+ ion in a resonant process. The decelerated electrons form the low-energy structure. For the CoRTC field that is used in our experiment, the ponderomotive energy is close to 5.2 eV. If the spacing of the $1s\sigma_g$ and the $2p\sigma_u$ state is higher than the ponderomotive energy of the electron, then energy exchange is very unlikely. This might explain why the low-energy elec-

trons vanish for KERs above 6 eV. The sharp edge at a KER of 3 eV and the almost complete absence of low-energy electrons for lower KERs is due to the fact that for these KERs resonant few-photon transitions between $1s\sigma_g$ and $2p\sigma_u$ are dominant (these are directly driven by the laser field). Another reason why for low KER there is no energy exchange of electron and ion is that low KER correspond to small spacings of $1s\sigma_g$ and $2p\sigma_u$, which are not resonant to the comparably high value of U_p .

V. CONCLUSION

In conclusion, we have studied the strong field dissociative ionization of molecular hydrogen. We observe a fingerprint of an energy exchange of the liberated electron with its parent molecular ion that occurs without recollision. We find that for certain internuclear distances the outgoing electron has an energy that is significantly lower than the ponderomotive energy. The apparently missing electron energy equals the energy spacing of the $1s\sigma_g$ and the $2p\sigma_u$ energy curve for the internuclear distance that corresponds to the measured KER of about 3.5 eV. We speculate that the electron might transfer some of its energy to the H_2^+ ion via a nonclassical antenna-like mechanism [52,53]. This is in line with our *ab initio* simulations that show a dependence of the

electron energy on the internuclear distance. Similar energy transfer mechanisms are known for single photon processes [54–56] but, so far, have not been observed in the strong field regime.

ACKNOWLEDGMENTS

The experimental work was supported by the DFG (German Research Foundation). We thank Reinhard Dörner for his support and fruitful discussions. O.N. gratefully acknowledges the support of the Alexander von Humboldt Foundation, and a Schmidt Science Fellowship. O.N., U.G., and A.R. acknowledge financial support from the European Research Council (ERC-2015-AdG-694097). The Flatiron Institute is a division of the Simons Foundation. This work was supported by the Cluster of Excellence Advanced Imaging of Matter (AIM), Grupos Consolidados (IT1249-19), and SFB925. L.S. acknowledges financial support from the Hungarian Scientific Research Fund (Grant No. K128621), the National Research, Development, and Innovation Office (Grant No. 2018-1.2.1-NKP-2018-00010), and the National Information Infrastructure Development Program. S.E. acknowledges funding of the DFG through Priority Programme SPP 1840 QUTIF.

-
- [1] L. V. Keldysh, Ionization in the field of a strong electromagnetic wave, *Sov. Phys. JETP* **20**, 1307 (1965).
- [2] P. B. Corkum, Plasma Perspective on Strong Field Multiphoton Ionization, *Phys. Rev. Lett.* **71**, 1994 (1993).
- [3] M. Lewenstein, P. Balcou, M. Y. Ivanov, A. L’Huillier, and P. B. Corkum, Theory of high-harmonic generation by low-frequency laser fields, *Phys. Rev. A* **49**, 2117 (1994).
- [4] J. L. Krause, K. J. Schafer, and K. C. Kulander, High-Order Harmonic Generation from Atoms and Ions in the High Intensity Regime, *Phys. Rev. Lett.* **68**, 3535 (1992).
- [5] W. Becker, B. N. Chichkov, and B. Wellegehausen, Schemes for the generation of circularly polarized high-order harmonics by two-color mixing, *Phys. Rev. A* **60**, 1721 (1999).
- [6] A. Fleischer, O. Kfir, T. Diskin, P. Sidorenko, and O. Cohen, Spin angular momentum and tunable polarization in high-harmonic generation, *Nat. Photonics* **8**, 543 (2014).
- [7] P. Lu, J. Wang, H. Li, K. Lin, X. Gong, Q. Song, Q. Ji, W. Zhang, J. Ma, H. Li, H. Zeng, F. He, and J. Wu, High-order above-threshold dissociation of molecules, *Proc. Natl. Acad. Sci.* **115**, 2049 (2018).
- [8] B. Walker, B. Sheehy, L. F. DiMauro, P. Agostini, K. J. Schafer, and K. C. Kulander, Precision Measurement of Strong Field Double Ionization of Helium, *Phys. Rev. Lett.* **73**, 1227 (1994).
- [9] S. Laroche, A. Talebpour, and L. S. Chin, Non-sequential multiple ionization of rare gas atoms in a ti:sapphire laser field, *J. Phys. B: At. Mol. Opt. Phys.* **31**, 1201 (1998).
- [10] B. Bergues, M. Kübel, N. G. Johnson, B. Fischer, N. Camus, K. J. Betsch, O. Herrwerth, A. Senfleben, A. M. Saylor, T. Rathje, T. Pfeifer, I. Ben-Itzhak, R. R. Jones, G. G. Paulus, F. Krausz, R. Moshhammer, J. Ullrich, and M. F. Kling, Attosecond tracing of correlated electron-emission in non-sequential double ionization, *Nat. Commun.* **3**, 813 (2012).
- [11] M. Kübel, K. J. Betsch, N. G. Kling, A. Alnaser, J. Schmidt, U. Kleineberg, Y. Deng, I. Ben-Itzhak, G. G. Paulus, T. Pfeifer, J. Ullrich, R. Moshhammer, M. Kling, and B. Bergues, Non-sequential double ionization of Ar: from the single- to the many-cycle regime, *New J. Phys.* **16**, 033008 (2014).
- [12] S. Eckart, M. Richter, M. Kunitski, A. Hartung, J. Rist, K. Henrichs, N. Schlott, H. Kang, T. Bauer, H. Sann, L. Ph. H. Schmidt, M. Schöffler, T. Jahnke, and R. Dörner, Nonsequential Double Ionization by Counterrotating Circularly Polarized Two-Color Laser Fields, *Phys. Rev. Lett.* **117**, 133202 (2016).
- [13] C. A. Mancuso, K. M. Dorney, D. D. Hickstein, J. L. Chaloupka, J. L. Ellis, F. J. Dollar, R. Knut, P. Grychtol, D. Zusin, C. Gentry, M. Gopalakrishnan, H. C. Kapteyn, and M. M. Murnane, Controlling Nonsequential Double Ionization in Two-Color Circularly Polarized Femtosecond Laser Fields, *Phys. Rev. Lett.* **117**, 133201 (2016).
- [14] A. S. Maxwell and C. F. d. M. Faria, Controlling Below-Threshold Nonsequential Double Ionization via Quantum Interference, *Phys. Rev. Lett.* **116**, 143001 (2016).
- [15] C. A. Mancuso, D. D. Hickstein, K. M. Dorney, J. L. Ellis, E. Hasović, R. Knut, P. Grychtol, C. Gentry, M. Gopalakrishnan, D. Zusin, F. J. Dollar, X.-M. Tong, D. B. Milošević, W. Becker, H. C. Kapteyn, and M. M. Murnane, Controlling electron-ion rescattering in two-color circularly polarized femtosecond laser fields, *Phys. Rev. A* **93**, 053406 (2016).
- [16] K. Lin, X. Jia, Z. Yu, F. He, J. Ma, H. Li, X. Gong, Q. Song, Q. Ji, W. Zhang, H. Li, P. Lu, H. Zeng, J. Chen, and J. Wu, Comparison Study of Strong-Field Ionization of Molecules and

- Atoms by Bicircular Two-Color Femtosecond Laser Pulses, *Phys. Rev. Lett.* **119**, 203202 (2017).
- [17] P. Eckle, A. N. Pfeiffer, C. Cirelli, A. Staudte, R. Dörner, H. G. Muller, M. Büttiker, and U. Keller, Attosecond ionization and tunneling delay time measurements in helium, *Science* **322**, 1525 (2008).
- [18] A. W. Bray, S. Eckart, and A. S. Kheifets, Keldysh-Rutherford Model for the Attoclock, *Phys. Rev. Lett.* **121**, 123201 (2018).
- [19] H. Ni, U. Saalman, and J.-M. Rost, Tunneling exit characteristics from classical backpropagation of an ionized electron wave packet, *Phys. Rev. A* **97**, 013426 (2018).
- [20] S. Eckart, K. Fehre, N. Eicke, A. Hartung, J. Rist, D. Trabert, N. Strenger, A. Pier, L. Ph. H. Schmidt, T. Jahnke, M. S. Schöffler, M. Lein, M. Kunitski, and R. Dörner, Direct Experimental Access to the Nonadiabatic Initial Momentum Offset upon Tunnel Ionization, *Phys. Rev. Lett.* **121**, 163202 (2018).
- [21] D. Trabert, S. Brennecke, K. Fehre, N. Anders, A. Geyer, S. Grundmann, M. Schöffler, L. Ph. H. Schmidt, T. Jahnke, R. Dörner, M. Kunitski, and S. Eckart, Angular dependence of the Wigner time delay upon tunnel ionization of H₂, *Nat. Commun.* **12**, 1697 (2021).
- [22] O. Jagutzki, A. Cerezo, A. Czasch, R. Dörner, M. Hattas, M. Huang, V. Mergel, U. Spillmann, K. Ullmann-Pfleger, T. Weber, H. Schmidt-Böcking, and G. D. W. Smith, Multiple hit readout of a microchannel plate detector with a three-layer delay-line anode, *IEEE Trans. Nucl. Sci.* **49**, 2477 (2002).
- [23] C. A. Mancuso, D. D. Hickstein, P. Grychtol, R. Knut, O. Kfir, X.-M. Tong, F. Dollar, D. Zusin, M. Gopalakrishnan, C. Gentry, E. Turgut, J. L. Ellis, M.-C. Chen, A. Fleischer, O. Cohen, H. C. Kapteyn, and M. M. Murnane, Strong-field ionization with two-color circularly polarized laser fields, *Phys. Rev. A* **91**, 031402(R) (2015).
- [24] Mancuso *et al.* used a total laser intensity between 1.7×10^{14} W/cm² and 3.0×10^{14} W/cm² with an intensity ratio I_{ω_0}/I_{ω} higher than 4 and observed a LES in the electron momentum distribution (see Fig. 11 in Ref. [15]). We used a total laser intensity of 0.87×10^{14} W/cm² and an intensity ratio of 1.6.
- [25] P. Agostini, F. Fabre, G. Mainfray, G. Petite, and N. K. Rahman, Free-Free Transitions Following Six-Photon Ionization of Xenon Atoms, *Phys. Rev. Lett.* **42**, 1127 (1979).
- [26] R. R. Freeman, P. H. Bucksbaum, H. Milchberg, S. Darack, D. Schumacher, and M. E. Geusic, Above-Threshold Ionization with Subpicosecond Laser Pulses, *Phys. Rev. Lett.* **59**, 1092 (1987).
- [27] G. Petite, P. Agostini, and H. Muller, Intensity dependence of non-perturbative above-threshold ionisation spectra: Experimental study, *J. Phys. B: At. Mol. Opt. Phys.* **21**, 4097 (1988).
- [28] J. Wu, M. Kunitski, M. Pitzer, F. Trinter, L. P. H. Schmidt, T. Jahnke, M. Magrakvelidze, C. B. Madsen, L. B. Madsen, U. Thumm, and R. Dörner, Electron-Nuclear Energy Sharing in Above-Threshold Multiphoton Dissociative Ionization of H₂, *Phys. Rev. Lett.* **111**, 023002 (2013).
- [29] W. Zhang, H. Li, K. Lin, P. Lu, X. Gong, Q. Song, Q. Ji, J. Ma, H. Li, H. Zeng, F. He, and J. Wu, Photon-number-resolved asymmetric dissociative single ionization of H₂, *Phys. Rev. A* **96**, 033405 (2017).
- [30] X. Sun, M. Li, Y. Shao, M.-M. Liu, X. Xie, Y. Deng, C. Wu, Q. Gong, and Y. Liu, Vibrationally resolved electron-nuclear energy sharing in above-threshold multiphoton dissociation of CO, *Phys. Rev. A* **94**, 013425 (2016).
- [31] W. Zhang, Z. Li, P. Lu, X. Gong, Q. Song, Q. Ji, K. Lin, J. Ma, F. He, H. Zeng, and J. Wu, Photon Energy Deposition in Strong-Field Single Ionization of Multielectron Molecules, *Phys. Rev. Lett.* **117**, 103002 (2016).
- [32] A. Staudte, D. Pavičić, S. Chelkowski, D. Zeidler, M. Meckel, H. Niikura, M. Schöffler, S. Schössler, B. Ulrich, P. P. Rajeev, T. Weber, T. Jahnke, D. M. Villeneuve, A. D. Bandrauk, C. L. Cocke, P. B. Corkum, and R. Dörner, Attosecond Strobing of Two-Surface Population Dynamics in Dissociating H₂⁺, *Phys. Rev. Lett.* **98**, 073003 (2007).
- [33] V. Hanus, S. Kangaparambil, S. Larimian, M. Dörner-Kirchner, X. Xie, M. S. Schöffler, G. G. Paulus, A. Baltuška, A. Staudte, and M. Kitzler-Zeiler, Subfemtosecond Tracing of Molecular Dynamics during Strong-Field Interaction, *Phys. Rev. Lett.* **123**, 263201 (2019).
- [34] V. Hanus, S. Kangaparambil, S. Larimian, M. Dörner-Kirchner, X. Xie, M. S. Schöffler, G. G. Paulus, A. Baltuška, A. Staudte, and M. Kitzler-Zeiler, Experimental Separation of Subcycle Ionization Bursts in Strong-Field Double Ionization of H₂, *Phys. Rev. Lett.* **124**, 103201 (2020).
- [35] L. Sarkadi, Laser-induced nonsequential double ionization of helium: classical model calculations, *J. Phys. B: At. Mol. Opt. Phys.* **53**, 165401 (2020).
- [36] L. Sarkadi, Comparative study of classical theoretical descriptions of the ionization of atoms induced by few-cycle laser pulses, *Phys. Rev. A* **103**, 053113 (2021).
- [37] M. Yu. Ivanov, M. Spanner, and O. Smirnova, Anatomy of strong field ionization, *J. Mod. Opt.* **52**, 165 (2005).
- [38] D. Trabert, N. Anders, S. Brennecke, M. S. Schöffler, T. Jahnke, L. P. H. Schmidt, M. Kunitski, M. Lein, R. Dörner, and S. Eckart, Nonadiabatic Strong Field Ionization of Atomic Hydrogen, *Phys. Rev. Lett.* **127**, 273201 (2021).
- [39] M. Marques, A. Rubio, E. K. Gross, K. Burke, F. Nogueira, and C. A. Ullrich, *Time-Dependent Density Functional Theory*, Vol. 706 (Springer Science & Business Media, Berlin, 2006).
- [40] C. Legrand, E. Suraud, and P.-G. Reinhard, Comparison of self-interaction-corrections for metal clusters, *J. Phys. B: At. Mol. Opt. Phys.* **35**, 1115 (2002).
- [41] X. Andrade, A. Castro, D. Zueco, J. Alonso, P. Echenique, F. Falceto, and A. Rubio, Modified ehrenfest formalism for efficient large-scale ab initio molecular dynamics, *J. Chem. Theory Comput.* **5**, 728 (2009).
- [42] L. Tao and A. Scrinzi, Photo-electron momentum spectra from minimal volumes: The time-dependent surface flux method, *New J. Phys.* **14**, 013021 (2012).
- [43] A. Scrinzi, t-surf: Fully differential two-electron photo-emission spectra, *New J. Phys.* **14**, 085008 (2012).
- [44] P. Wopperer, U. De Giovannini, and A. Rubio, Efficient and accurate modeling of electron photoemission in nanostructures with tddft, *Eur. Phys. J. B* **90**, 51 (2017).
- [45] A. Castro, H. Appel, M. Oliveira, C. A. Rozzi, X. Andrade, F. Lorenzen, M. A. Marques, E. Gross, and A. Rubio, Octopus: a tool for the application of time-dependent density functional theory, *Phys. Stat. Sol. (b)* **243**, 2465 (2006).
- [46] X. Andrade, D. Strubbe, U. De Giovannini, A. H. Larsen, M. J. Oliveira, J. Alberdi-Rodriguez, A. Varas, I. Theophilou, N. Helbig, M. J. Verstraete *et al.*, Real-space grids and the octopus code as tools for the development of new simulation approaches

- for electronic systems, *Phys. Chem. Chem. Phys.* **17**, 31371 (2015).
- [47] N. Tancogne-Dejean, M. J. Oliveira, X. Andrade, H. Appel, C. H. Borca, G. Le Breton, F. Buchholz, A. Castro, S. Corni, A. A. Correa *et al.*, Octopus, a computational framework for exploring light-driven phenomena and quantum dynamics in extended and finite systems, *J. Chem. Phys.* **152**, 124119 (2020).
- [48] O. Neufeld and O. Cohen, Background-Free Measurement of Ring Currents by Symmetry-Breaking High-Harmonic Spectroscopy, *Phys. Rev. Lett.* **123**, 103202 (2019).
- [49] A. Giusti-Suzor, X. He, O. Atabek, and F. H. Mies, Above-Threshold Dissociation of H_2^+ in Intense Laser Fields, *Phys. Rev. Lett.* **64**, 515 (1990).
- [50] K. Harumiya, H. Kono, Y. Fujimura, I. Kawata, and A. D. Bandrauk, Intense laser-field ionization of H_2 enhanced by two-electron dynamics, *Phys. Rev. A* **66**, 043403 (2002).
- [51] L. Cattaneo, J. Vos, R. Y. Bello, A. Palacios, S. Heuser, L. Pedrelli, M. Lucchini, C. Cirelli, F. Martín, and U. Keller, Attosecond coupled electron and nuclear dynamics in dissociative ionization of H_2 , *Nat. Phys.* **14**, 733 (2018).
- [52] M. Y. Kuchiev, Atomic antenna, *Sov. Phys. JETP* **45**, 404 (1987).
- [53] M. Y. Kuchiev, ATI as a source for multiply charged ion production in a laser field, *J. Phys. B: At. Mol. Opt. Phys.* **28**, 5093 (1995).
- [54] L. S. Cederbaum, J. Zobeley, and F. Tarantelli, Giant Intermolecular Decay and Fragmentation of Clusters, *Phys. Rev. Lett.* **79**, 4778 (1997).
- [55] T. Jahnke, A. Czasch, M. S. Schöffler, S. Schössler, A. Knapp, M. Kász, J. Titze, C. Wimmer, K. Kreidi, R. E. Grisenti, A. Staudte, O. Jagutzki, U. Hergenhahn, H. Schmidt-Böcking, and R. Dörner, Experimental Observation of Interatomic Coulombic Decay in Neon Dimers, *Phys. Rev. Lett.* **93**, 163401 (2004).
- [56] L. S. Cederbaum, Fragmentation of molecules by virtual photons from remote neighbors, *J. Phys. Chem. Lett.* **11**, 8964 (2020).